Informatics in Medicine Unlocked 17 (2019) 100256

Contents lists available at ScienceDirect

Informatics in Medicine Unlocked

journal homepage: http://www.elsevier.com/locate/imu

Automated grading of prostate cancer using convolutional neural network and ordinal class classifier

Bejoy Abraham [a,b,*], Madhu S. Nair [c]

[a] Department of Computer Science, University of Kerala, Kariavattom, Thiruvananthapuram, 695581, Kerala, India
[b] Department of Computer Science and Engineering, College of Engineering Perumon, Kollam, 691601, Kerala, India
[c] Artificial Intelligence & Computer Vision Lab, Department of Computer Science, Cochin University of Science and Technology, Kochi, 682022, Kerala, India

ARTICLE INFO

Keywords:
Ordinal class classifier
CNN
Gleason grading
Prostate cancer
Computer-aided diagnosis

ABSTRACT

Prostate Cancer (PCa) is one of the most prominent cancer among men. Early diagnosis and treatment planning are significant in reducing the mortality rate due to PCa. Accurate prediction of grade is required to ensure prompt treatment for cancer. Grading of prostate cancer can be considered as an ordinal class classification problem. This paper presents a novel method for the grading of prostate cancer from multiparametric magnetic resonance images using VGG-16 Convolutional Neural Network and Ordinal Class Classifier with J48 as the base classifier. Multiparametric magnetic resonance images of the PROSTATEx-2 2017 grand challenge dataset are employed for this work. The method achieved a moderate quadratic weighted kappa score of 0.4727 in the grading of PCa into 5 grade groups, which is higher than state-of-the-art methods. The method also achieved a positive predictive value of 0.9079 in predicting clinically significant prostate cancer.

1. Introduction

Prostate Cancer (PCa) is the most prominent cancer among men, next only to lung cancer. It is estimated that there will be nearly 1,74,650 of new incidences and 31,620 prostate cancer-related deaths in the United States during 2019. PCa accounts for nearly 1 in 5 new cancer diagnoses among men [1]. Early diagnosis and treatment planning is significant in reducing the mortality rate due to PCa.

The Gleason Score (GS) is a standard for measuring the aggressiveness of Prostate cancer. The Gleason Score is the sum of two Gleason grades that are most common in a lesion pattern [2]. The pathologist assigns a Gleason grade on a scale of 3–5 based on the pattern of cancer cells in the prostate. PCa is divided into 5 different grade groups based on the Gleason Score [3]. Gleason Score $<= 6$ are categorized into Grade Group (GG) 1 and a Gleason Score ≥ 7 is categorized into GG 2 (GS $3 + 4 = 7$), GG 3 (*GS* $4 + 3 = 7$), GG 4 (GS $4 + 4 = 8$, GS $3 + 5 = 8$, GS $5 + 3 = 8$) and GG 5 (GS $= 9$, GS $= 10$) based on cancer aggressiveness [4]. Doctors predict the prospect of recovery based on the grade group [4]. Lesions categorized as GG 1 are considered clinically insignificant and those categorized as GG 2, GG 3, GG 4 and GG 5 are considered clinically significant [5]. No treatment is required for clinically insignificant cancer, but active surveillance is needed [6]. Accurate prediction of grade is required to prevent overtreatment of clinically insignificant tumors and to ensure prompt treatment for clinically significant prostate cancer [7].

Screening of PCa is done using Digital Rectal Examination (DRE), estimating Prostate Specific Antigen (PSA) level and Transrectal Ultrasound (TRUS) biopsy [8]. Histopathologic verification is used for confirming the diagnosis [8]. Treatment planning is done based on the grade group of a lesion assigned by the pathologist based on the microscopic examination of histological images [9]. TRUS biopsy often leads to over-diagnosis of clinically insignificant cancers, and poor-diagnosis of clinically significant ones [10]. Recent studies show that MRI can be used for the diagnosis as well as the grading of PCa [11,12]. Computer-aided diagnosis techniques could assist the radiol-ogist in estimating the grade of PCa from MRI, which is time-consuming and stressful if done manually.

Few recent studies perform computer-aided classification between clinically significant and clinically insignificant PCa. A pioneering method for classification of clinically-significant and clinically insignificant PCa was done by Fehr et al. [13]. The method utilized texture feature, RFE-SVM classifier and SMOTE based upsampling of instances in minority classes. Subsequently, the International Society for Optics and Photonics (SPIE) along with the American Association of Physicists

* Corresponding author. Department of Computer Science, University of Kerala, Kariavattom, Thiruvananthapuram, 695581, Kerala, India.
E-mail address: bjoyabraham@gmail.com (B. Abraham).

https://doi.org/10.1016/j.imu.2019.100256
Received 28 August 2019; Received in revised form 29 September 2019; Accepted 14 October 2019
Available online 15 October 2019

in Medicine (AAPM) and the National Cancer Institute (NCI) organized a grand challenge for the classification of clinically-significant and indolent lesions [14]. Methods by Seah et al. [15] and Liu et al. [16] used Convolutional Neural Networks and Kitchen et al. [17] used SVM to achieve significant results in the PROSTATEx test dataset. The methods by Le et al. [18] and Wang et al. [19] using Convolutional Neural Networks achieved good performance using the training dataset of the challenge along with a private dataset. Abraham et al. [20] used features extracted using sparse autoencoders and the random forest classifier to distinguish between clinically significant and clinically insignificant Pca, using the training dataset of PROSTATEx, after balancing instances using ADASYN.

Following the PROSTATEx challenge, AAPM, SPIE, and NCI conducted PROSTATEx-2 grand challenge for the grading of PCa into 5 grade groups [14]. The method submitted by the authors won the challenge, achieving a Quadratic Weighted Kappa value of 0.2772 [21] in the highly imbalanced PROSTATEx-2 dataset. The method also achieved a positive predictive value $PPV_{GG>1}$ of 0.80 in predicting clinically significant prostate cancer. The method used texture features as input and produced deep features using a stacked sparse autoencoder [21]. In a recent work, the authors used the Inception-V3 pre-trained network and LADTree classifier to achieve a *fair* quadratic weighted kappa score [22]. In another study, Jensen et al. [23] performed binary classification of GG1, GG2, GG (1 + 2), GG 3 and GG (4 + 5) to achieve significant results using image histogram and texture features in combination with the *k*-nearest neighbor classifier. However, instead of multi-class classification into 5 grade groups, they have combined the GG 4 and GG 5 of PROSTATEx-2 datasets and performed classification of GG (4 + 5) as a separate category. As the grading of prostate cancer into 5 grade groups from MR images is a relatively new area of research, there exist only a few published works in this area. The published works in the literature for the grading of prostate cancer into 5 grade groups from MRI are those described in Refs. [21,22].

The above-mentioned works have few limitations worth mentioning. Most of the existing techniques [15–20] are able to distinguish between high-grade and low-grade PCa only, and not between all of the 5 grade groups. Even though the winning method of PROSTATEx-2 challenge achieved a *fair* quadratic weighted kappa score, it was unable to predict any cancer belonging to GG 4 [21]. The subsequent method was unable to predict any lesion belonging to GG 5. The method described in Ref. [23] performed classification of prostate cancer into different grade groups after combining GG 4 and GG 5 only. No existing methods have reported a *moderate* quadratic weighted kappa score above 0.40.

None of the existing works considered the ordinal nature of the grading problem. State-of-the-art techniques have used Convolutional Neural Network (CNN) [24], Support Vector Machine (SVM) [18], Softmax [21], and LADTree [22] for classification of ordinal prostate cancer data. However, a number of works in the literature have shown that the Ordinal Class Classifier (OCC) is effective in the classification of imbalanced classification problems of ordinal nature. Perez et al. [25] used the Ordinal Class Classifier for the classification of highly imbalanced melanoma images of ordinal nature. Cardoso et al. [26] used OCC for the aesthetic evaluation of breast cancer conservative treatment. The proposed method explores the use of OCC in combination with high-level features extracted from CNN for the grading of PCa.

The proposed method has the following contributions.

1. The method is the first one in the literature to use the combination of VGG-16 pre-trained CNN along with OCC for PCa diagnosis.
2. Even though there exist several methods for predicting clinically significant PCa using binary classification, this method is one among the few to perform multi-class classification for predicting clinically significant PCa.
3. The method is the first one in the literature to achieve a *moderate* quadratic weighted kappa score using the PROSTATEx-2 challenge dataset.

The remainder of the paper is organized as follows. Section 2 describes the materials and methods used in this study. Dataset, preprocessing, feature extraction technique and classifier used for the study are described in detail in this section. Results and experimental analysis are explained in Section 3. Section 4 describes the conclusions of the study.

2. Materials and methods

2.1. Dataset

A publicly available dataset, PROSTATEx-2 (train), which was earlier used as the training dataset of the PROSTATEx-2 2017 challenge, has been utilized in this study. An expert radiologist identified suspicious lesions in each MRI and assigned a PI-RADS score [14]. Findings with a PI-RADS score >= 3 were subjected to magnetic resonance guided biopsy, and graded thereupon by a pathologist. These outcomes were used as the ground truth [14]. T2W, high B-Value DWI (HBVAL) and ADC images from the dataset are employed for the work. Fig. 1 illustrates the 5 grade groups in ADC, HBVAL and T2W images.

Thirty-six lesions of GG 1, 41 lesions of GG 2, 20 lesions of GG 3, 8 lesions of GG 4, and 7 lesions of GG 5 were present. The dataset is available in the Cancer Imaging Archive (TCIA) [27–29]. The test dataset of the challenge could not be incorporated, as its ground truth is not made public yet. To overcome this limitation, we have performed cross-validations on the PROSTATEx-2 training dataset, after dividing it into training and test sets.

2.2. Pre-processing

Ground truth of the PROSTATEx-2 dataset is a (p, q, r) coordinate voxel point roughly placed at the tumor's center [22]. Similar to the method in Ref. [22], a region of interest (ROI) of size $15 \times 15 \times 3$ surrounding the ground truth was selected from HBVAL and ADC MRI volumes, and an ROI of dimension $60 \times 60 \times 3$ surrounding the ground truth was selected from T2W images. Three contiguous slices were chosen, which is represented by 3 in the ROI size. The dimension of T2W varies from that of the other modalities, due to the image acquisition resolution [22]. A volume of dimension $224 \times 224 \times 3$ was prepared from each of the ADC, HBVAL, and T2W images. The method and program by Vallieres et al. [30] were used for generating the volumes. Slice spacing of each volume was set to 1 mm, the scale at which a volume is

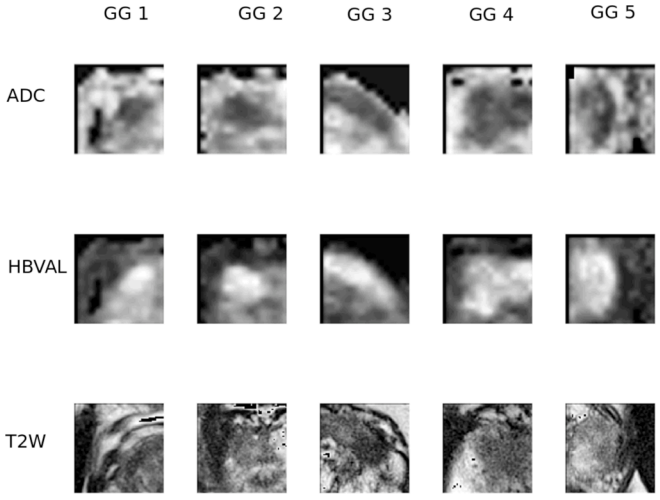

Fig. 1. The figure corresponds to sample images of GG 1, GG 2, GG 3, GG 4, and GG 5. First, second and third rows represent ADC, HBVAL, and T2W images, whereas first, second, third, fourth, and fifth columns represent GG 1, GG 2, GG 3, GG 4, and GG 5.

isotropically resampled was set to 1 mm, the quantization algorithm was set to the Lloyd-Max quantization algorithm, and the number of grey levels in the quantization process was set to 32. T2W images were acquired using a different in-plane resolution, as compared to ADC and HBVAL images. Due to this difference, in-plane resolution of the volume of interest was set to 3.8 mm for T2W and 14.9 mm for ADC and HBVAL images. Fig. 2 illustrates the generation of ROI from ADC, HBVAL, and T2W images.

2.3. Feature extraction using VGG-16

A Convolutional Neural Network can be used to learn the hierarchy of sophisticated features in different layers. The traditional CNN consists of convolutional, pooling, activation and fully-connected layers. A convolution function describes an operation on two functions. One function consists of voxel values at a position in the volumetric image, and the second function is a kernel. The dot product between the two functions produces the output. The kernel is then shifted to the next position in the volumetric image based on the stride specified. The computation is repeated until the entire volume is covered, producing a feature activation map. The convolution function is defined as

$$(h_j)_{mn} = (W_j * y)_{mn} + b_j \quad (1)$$

Where $j = 1, \ldots, J$ is the index of the jth feature map in the convolution layer, and m, n is the index of neuron s in the jth feature map, W_j is the weight and b_j corresponds to the bias of jth kernel, and y represents the input and (h_j) is the output corresponding to the jth feature map.

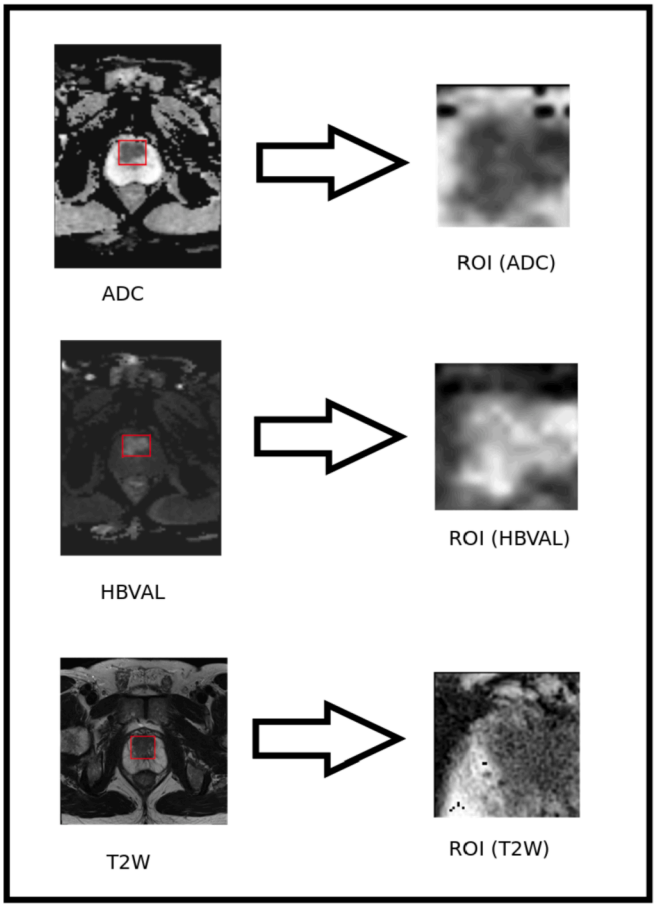

Fig. 2. The figure corresponds to the image ProstateX-0026 in the dataset. The ground truth of ADC and HBVAL images were (38, 66, 5) and that of T2W was (175, 197, 6). An ROI of size $15 \times 15 \times 3$ surrounding the ground truth was selected from ADC and HBVAL images and an ROI of size $60 \times 60 \times 3$ was selected from T2W images. We have indicated the region containing the lesion in red color.

The output from the convolutional layer is passed to an activation layer. The most common activation function is the Rectified Linear Units (ReLU) function, a non-linear activation function which converts negative input to zero [31]. The ReLU function accelerates the computation and training, and solves the vanishing of gradient issue. The ReLU function is defined as

$$f(t) = maximum(0, t) \quad (2)$$

Where t is the input to the neuron. Other major activation functions are sigmoid, Softmax and tanh functions.

The Pooling Layer is a nonlinear subsampling layer which downsamples the image by taking mean or maximum values over a neighborhood of the input feature maps. The most common type of pooling is max-pooling which introduces translation invariance to deformations and minor shifts in the feature maps. The max-pooling merges semantically similar features, thereby reducing the dimension of the feature maps.

The last layer of the convolutional neural network is a Fully Connected (FC) layer. All neurons in the preceding layer are linked to all neurons in the fully-connected layer. There can be one or more fully-connected layers based on the level of feature abstraction required [31].

As CNN maintain spatial relationships, they are suitable to perform object recognition tasks. Training a CNN from scratch requires a massive amount of annotated data which is hard to obtain for medical imaging. In such instances, pre-trained off-the-shelf networks trained in a large dataset such as ImageNet [32] can be used for feature extraction [33].

The VGG-16 pre-trained CNN is used for this study. VGG-16, proposed by Simonyan et al. [34], is the architecture that won the ImageNet Large Scale Visual Recognition Challenge 2014 (ILSVRC2014) in the localization and classification categories. Simonyan et al. [34] observed that using small convolution kernels of size 3×3 throughout the network allows coarse-to-fine image patterns to be recognized, which leads to improved generalization. VGG-16 was earlier used for several medical imaging applications including skin lesion segmentation [35] and iris recognition [33]. It consists of 13 convolution layers of filter size 3×3 and 5 max-pooling layers of size 2×2. It also consists of Rectified linear units (ReLU) and dropout units, which are used to check overfitting. Three fully-connected layers are present in VGG-16 networks. Features are extracted from the last fully-connected layer of the network. ROI of size $224 \times 224 \times 3$ generated from ADC, HBVAL and T2W images are passed as input to the VGG-16 network. VGG-16 constructs a hierarchical representation of input images. Deeper layers contain higher-level features, generated using the lower-level features of preceding layers. To obtain the feature representations of the input images, activations are applied on the last fully connected layer consisting of 1000 neurons. Three feature vectors of dimension 112×1000 each are constructed from ADC, HBVAL, and T2W images. A feature vector of size 112×3000 is produced by concatenating the above-mentioned feature vectors. Principal Component Analysis (PCA) is used to bring down the size of the feature vector to 112×32. Dimensionality reduction is achieved by choosing enough eigenvectors to account for 85% of the variance in the original data. 32 eigenvectors are chosen by the PCA algorithm implemented in WEKA. PCA is applied to the feature vector extracted from the whole dataset. However, it is worth noting that PCA performed on the entire dataset could be less ideal as compared with PCA performed on the training set and applying the transformation on the test set. No other pre-processing techniques are employed while applying PCA.

2.4. Classification

Grading of prostate cancer can be considered as an ordinal class classification problem. Let G1, G2, G3, G4, and G5 be the different grade

groups. The grades can be ordered in the increasing order of aggressiveness as $G1 < G2 < G3 < G4 < G5$. Normal classifiers cannot recognize this ordering information. An ordinal class classifier enables a normal base classifier to utilize the ordering information provided in the class attributes [36]. We used an Ordinal Class Classifier associated with WEKA as the classifier for the proposed technique. The Ordinal Class Classifier is a meta-classifier which permits application of conventional classification techniques to ordinal class problems [36]. The data corresponding to the n-class ordinal problem is reconstructed into a n - 1 binary problem. For each of the n - 1 binary attributes, a new dataset is extracted during the training process [36]. Subsequently, the base classifier is tried, to obtain a model corresponding to each of the newly generated datasets.

Let G_i be the class values. The probability of a sample belonging to the first ordinal class is

$$P(G_1) = 1 - P(Target > G_1) \tag{3}$$

The probability of an instance belonging to jth ordinal class is given by

$$P(G_j) = P(Target > G_{j-1}) \times (1 - P(Target > G_j)),\ 1 < j < n \tag{4}$$

The probability of the last ordinal class is given by

$$P(G_n) = P(Target > G_{n-1}) \tag{5}$$

During testing, an unknown sample is dealt by all among the n - 1 classifiers, and the probability of each among the n ordinal category is estimated using the aforementioned technique. The class with the highest probability is assigned to the unknown sample [36].

We used J48 as the base classifier. J48 is a class for creating a pruned or unpruned C4.5 binary decision tree [37]. Nodes of C4.5 decision tree represents features, branches represent values of features, and leaf represents classes. At each node of the tree, the attribute with highest information gain is selected, which divides its set of samples into different subsets. J48 iteratively traverses each node to determine the best division. If all samples in a subset correspond to the same class, the division process terminates. A leaf node is constructed in the decision tree corresponding to the selected class. The confidence factor, the minimum number of objects, number of folds, and seed of J48 were set as 0.25, 1, 3, and 1, respectively.

The architecture of the proposed technique is illustrated in Fig. 3.

3. Results and discussion

The quadratic weighted kappa score [38,39] was the performance measure used in the PROSTATEx-2 challenge for measuring the performance of various methods. The kappa score is calculated as

$$K = (P_{oa} - P_{ca})/(1 - P_{ca}) \tag{6}$$

Where P_{oa} is the proportion of observed agreements, and P_{ca} is the proportion of chance agreements. A quadratic weighted kappa reflects the degree of disagreement, in such a way that more emphasis is given to bigger differences among ratings than to minor differences [40]. The quadratic weighted kappa is suitable for multicategory ordinal class classification [40]. It is a suitable performance metric for extremely disproportioned data [41] as in PROSTATEx-2, whereas accuracy is a misleading performance measure in such cases [4221], as it does not take into account prevalence of the disease in various grade groups. The 95% Confidence Interval (CI) for proportions are computed according to the Wilson efficient-score method, corrected for continuity. The result is considered statistically significant if zero is not included in the 95% CI. A Chi-square based p-value is further computed for results whose 95% CI does not include zero for ascertaining the statistical significance. The result is considered statistically significant if the p-value is less than 0.05.

In addition to the quadratic weighted kappa score, positive predictive value (PPV) in predicting clinically significant cancers ($PPV_{GG>1}$) was used as the additional performance metric in the PROSTATEx-2 challenge.

$$PPV_{GG>1} = CP_{GG>1}/T_{GG>1} \tag{7}$$

Where $CP_{GG>1}$ is the number of instances of $GG > 1$ correctly predicted as $GG > 1$ and $T_{GG>1}$ is the total instances of $GG > 1$.

The quadratic weighted kappa score ranges from −1 to +1 and is interpreted as *poor*, *slight*, *fair*, *moderate*, *substantial,* and *almost perfect* based on its magnitude. Table 1 shows the interpretation of the different range of quadratic weighted kappa scores [39].

Implementation of the method is done using MATLAB 2018b on a WINDOWS 10 platform, with an Intel (R) core (TM) i7-7700 HQ CPU at 2.81 Ghz with 16 GB RAM and NVIDIA GTX 1060 6 GB GPU.

A Leave-One-Patient-Out (LOPO) cross-validation was performed on the PROSTATEx- 2(train) dataset. A *moderate* quadratic weighted kappa score of 0.4727 and 95% CI of [0.27755, 0.66785] was reached. The p-

Table 1
Interpretation of quadratic weighted kappa.

Sl. No	Range of Quadratic Weighted Kappa	Concordance
1	Negative	poor
2	0.01–0.20	slight
3	0.21–0.40	fair
4	0.41–0.60	moderate
5	0.61–0.80	substantial
6	0.81–1	almost perfect

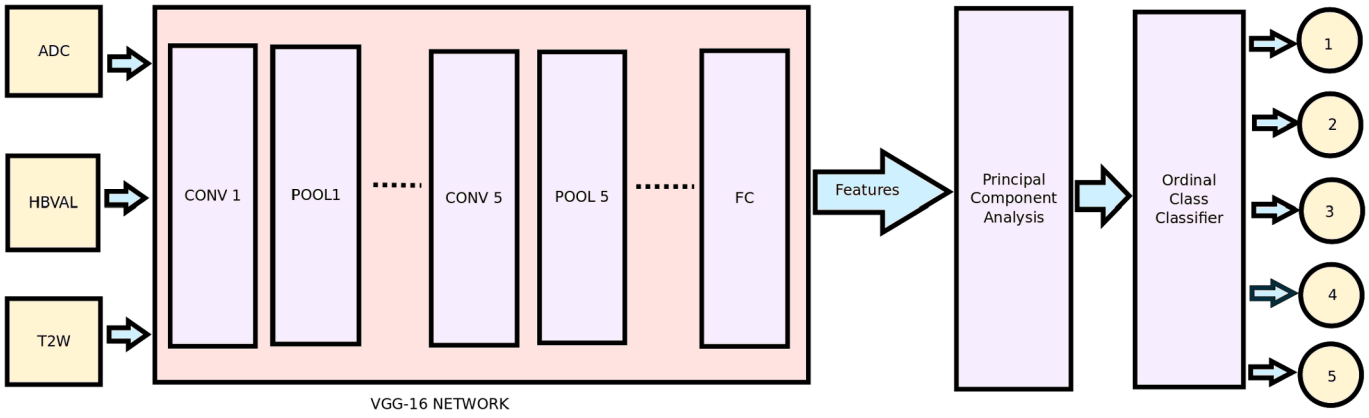

Fig. 3. Architecture of the proposed method. Input volumes are given to a VGG-16 pre-trained network for feature extraction. The extracted features from the fully-connected (FC) layer are given as input to an ordinal class classifier for grading.

value was further computed with the significance level set to 0.05. A p-value of <0.001 was attained, which is significant. Table 2 displays the consolidated result. The confusion matrix corresponding to the result is shown in Fig. 4.

The method was able to categorize prostate cancer belonging to GG 1, GG 2, and GG 5 with moderate precision and recall. The correctly classified instances were comparatively less for GG 4. One reason for less accurate predictions for GG 4 is the fewer number of training samples belonging to the class. However, it is worth noting that none of the GG 4 tumors was misclassified as clinically insignificant ones. All of the GG 4 lesions were correctly classified as clinically significant. It is also observed that only one among the seven GG 5 lesions was wrongly classified as clinically insignificant. The method achieved a $PPV_{GG>1}$ of 0.9079 in distinguishing low-grade PCa from high-grade PCa. The diagnostic accuracy achieved was 47.32%.

To evaluate the performance per grade group, we considered proportions of agreement within each of the 5 grade groups separately. Proportions of agreement achieved are given in Table 3. Grade groups 3 and 4 could achieve proportions of agreement less than 0.2 only whereas grade groups 2 and 5 achieved *fair* proportions of agreement between 0.2 and 0.4. Grade group 1 achieved a *moderate* proportion of agreement greater than 0.4. In addition to the proportions of agreement, we have also computed precision, recall, and Area under the Receiver Operating Characteristic Curve (AUC), achieved per grade group, which is represented in Table 4.

Performance of VGG-16 pre-trained network was compared with that of other networks, and the result is shown in Table 5. No networks other than VGG-16 reached a *moderate* quadratic weighted kappa score. DenseNet and InceptionResnet-V2 could achieve only a *poor* quadratic weighted kappa score. SqueezeNet, ResNet-50, ResNet- 101, VGG-19 and Inception-V3 achieved a *slight* quadratic weighted kappa in combination with OCC. Only the proposed network and Inception-V3 was able to achieve a statistically significant quadratic weighted kappa score, where 95% CI does not include zero. The p-value was further computed for the results achieved using Inception-V3 and VGG-16. The methods achieved a p-value of 0.0132 and < 0.001 respectively, which are significant.

The performance of the Ordinal Class Classifier was compared with that of several other classifiers. Features extracted using the VGG-16 network, along with default parameter settings of the classifiers, were used for the comparison shown in Table 6. OCC attained a *moderate* quadratic weighted kappa score, whereas other classifiers could achieve a *fair*, *slight* or *poor* quadratic weighted kappa score only. PART, OneR, Logistic, DMNBtext, END, FT, JRip, NNge, VFI, Classification via Regression, Naive- Bayes, NBTree, and KStar achieved a *slight* quadratic weighted kappa score. IB1, Log- ITBoost, MultiClass Classifier, IBK and Multilayer Perceptron achieved a *fair* quadratic weighted kappa score. OCC, IB1, LogitBoost, MultiClass Classifier, IBK, and Multilayer Perceptron achieved statistically significant results based on both 95% CI and p-value.

Performance of J48 as the base classifier for OCC was evaluated along with other major decision tree based classifiers. Table 7 displays the comparison of various decision tree based classifiers used as the base classifier of OCC. ADTree, FT, J48graft, and Random Tree achieved a *fair* quadratic weighted kappa score. BFTree, LMT, NBTree, Simple Cart, and Random Forest achieved a *slight* quadratic weighted kappa score. Decision Stump was able to achieve a *poor* quadratic weighted kappa score

Table 2
Results: Quadratic weighted kappa, $PPV_{GG>1}$, standard error, 95% CI and P-value.

Quadratic Weighted Kappa	$PPV_{GG>1}$	Standard Error	95% CI	P-value
0.4727	0.9079	0.09957	[0.27755, 0.66785]	$2.333e^{-8}$

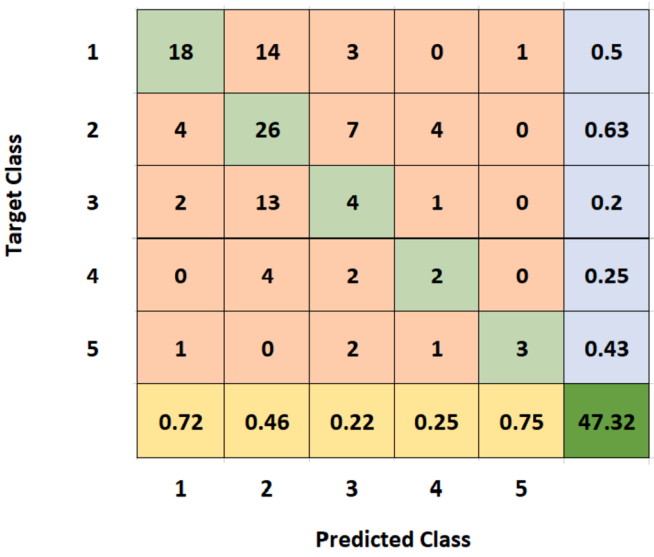

Fig. 4. Confusion Matrix. Element in the bottom-right corner corresponds to accuracy. Bottom row represents precision and rightmost column corresponds to recall. Consider rows from 2 to 5. Among the 76 clinically significant instances, 69 are classified as clinically significant. $PPV_{GG>1} = 69/76 = 0.9079$.

Table 3
Proportions of agreement (PoA) corresponding to each grade group.

GG	Observed PoA	95% CI
1	0.4186	[0.2737 to 0.5779]
2	0.3611	[0.2537 to 0.4835]
3	0.1176	[0.0384 to 0.2839]
4	0.1429	[0.0251 to 0.4385]
5	0.375	[0.1024 to 0.7411]

Table 4
Precision, recall and AUC per grade group.

GG	Precision	Recall	AUC
1	0.72	0.5	0.626
2	0.456	0.634	0.535
3	0.222	0.2	0.379
4	0.25	0.25	0.761
5	0.75	0.429	0.847

Table 5
Performance comparison of pre-trained networks.

Sl. No	Network	Quadratic Weighted Kappa	95% CI	P-value
1	DenseNet	−0.04714	[-0.21822 to 0.12393]	–
2	SqueezeNet	0.03549	[-0.13400, 0.20497]	–
3	ResNet-50	0.15044	[-0.02168 to 0.32256]	–
4	ResNet-101	0.00207	[-0.15306 to 0.15720]	–
5	InceptionResnet-V2	−0.12426	[-0.28548 to 0.03696]	–
6	VGG-19	0.14118	[-0.01399 to 0.29634]	–
7	Inception-V3	0.19882	[0.00235 to 0.39529]	0.0132
8	VGG-16	0.4727	[0.27755 to 0.66785]	<0.001

Table 6
Performance comparison of classifiers.

Sl. No	Classifier	Quadratic Weighted Kappa	95% CI	P-value
1	PART	0.08832	[-0.13338 to 0.31001]	–
2	OneR	0.00329	[-0.14464 to 0.15123]	–
3	IB1	0.32377	[0.14756 to 0.49998]	0.0019
4	RBF Network	−0.01186	[-0.16890 to 0.14518]	–
5	Logistic	0.14565	[-0.01369 to 0.30500]	–
6	DMNBtext	0.06864	[-0.06335 to 0.20064]	–
7	AdaBoost	−0.14056	[-0.25726 to −0.02387]	–
8	END	0.17455	[-0.06620 to 0.41529]	–
9	LogitBoost	0.28564	[0.10126 to 0.47001]	0.0464
10	MultiBoostAB	−0.14056	[-0.25726 to −0.02387]	–
11	FT	0.17116	[0.01301 to 0.32931]	0.0830
12	Simple Cart	−0.01514	[-0.11167 to 0.08139]	–
13	JRip	0.10736	[-0.03629 to 0.25101]	–
14	NNge	0.05421	[-0.05671 to 0.16513]	–
15	VFI	0.14962	[-0.02514 to 0.32438]	–
16	Classification Via Regression	0.11244	[-0.06600 to 0.29089]	–
17	Classification Via Clustering	−0.02294	[-0.13438 to 0.08851]	–
18	Decorate	−0.08538	[-0.25201 to 0.08124]	–
19	MultiClass Classifier	0.23839	[0.07903 to 0.39775]	0.0237
20	IBK	0.32377	[0.14756 to 0.49998]	0.0019
21	Multilayer Perceptron	0.23332	[0.07177 to 0.39487]	0.0244
22	Naïve Bayes	0.11878	[-0.05699 to 0.29455]	–
23	NBTree	0.09100	[-0.13819 to 0.32019]	–
24	KStar	0.19706	[0.03623 to 0.35788]	0.1437
25	Ordinal Class Classifier	0.4727	[0.27755 to 0.66785]	<0.001

Table 7
Comparison of base classifiers.

Sl. No	Classifier	Quadratic Weighted Kappa	95% CI	P-value
1	ADTree	0.21066	[-0.00193 to 0.42324]	–
2	BFTree	0.05823	[-0.10438 to 0.22085]	–
3	Decision Stump	−0.10400	[-0.27598 to 0.06798]	–
4	FT	0.26041	[0.11606 to 0.40476]	0.032868
5	J48graft	0.35358	[0.16656 to 0.54060]	<0.001
6	LMT	0.03352	[-0.11006 to 0.17710]	–
7	NBTree	0.14400	[-0.05513 to 0.34312]	–
8	Random Forest	0.06413	[-0.06423 to 0.19250]	–
9	Random Tree	0.21919	[0.01572 to 0.42266]	0.019944
10	Simple Cart	0.00267	[-0.10799 to 0.11333]	–
11	J48	0.47270	[0.27755 to 0.66785]	<0.001

only. The J48 classifier was able to achieve a *moderate* quadratic weighted kappa score. J48, FT, J48graft, and Random Tree achieved a statistically significant result whose 95% CI does not include zeros and p-value<0.05. No other base classifier was able to achieve a statistically significant result.

Table 8 displays the comparison of various methods in the literature for the grading of PCa. 95% CI is mentioned in the table only if the same is reported in respective papers. Most of the techniques have either used PROSTATEx-1 or PROSTATEx-2 datasets. AUC was the performance measure used in the PROSTATEx-1 challenge for the binary classification of low-grade and high-grade prostate cancer, whereas the quadratic weighted kappa is the performance measure used in the PROSTATEx-2 challenge for the grading of prostate cancer into 5 grade groups. The proposed method achieved a *moderate* quadratic weighted kappa score of 0.4727 whereas the previous method by the authors, which won the PROSTATEx-2 2017 challenge, could achieve a *fair* quadratic weighted kappa score only. The proposed method was also able to predict high-grade PCa with a $PPV_{GG>1}$ of 0.9079. The proposed method broke the null hypothesis as it achieved a 95% CI of [0.27755, 0.66785]. The quadratic weighted kappa scores achieved by the 43 methods participated in the PROSTATEx-2 challenge range from −0.24 to 0.2772, and none of the methods could achieve a *moderate* quadratic weighted kappa score greater than 0.40 [14]. Le et al. [18] used a combination of PROSTATEx-1(train) and a private dataset named TJPCa to achieve a significant AUC of 0.909. Even though the methods by Le et al. [18] and Wang et al. [19] achieved significant AUC in distinguishing low-grade and high-grade PCa, their methods do not perform classification for all of the 5 grade groups. Their methods perform classification of PCa with $GG = 1$ vs. $GG >= 2$ only. Jensen et al. [23] performed a binary classification of GG1, GG2, GG (1 + 2), GG 3 and GG (4 + 5) to achieve AUC of 0.85, 0.89, 0.83, 0.94 and 0.86 respectively. Instead of multi-class classification of 5 grade groups, they have performed classification of GG (4 + 5) as a separate category, since the number of subjects belonging to these two grade groups are considerably less. Another method by the authors achieved a $PPV_{GG>1}$ of 0.8158, a quadratic weighted kappa score of 0.3772, and a 95% CI of [0.2111, 0.5433] [22] for the PROSTATEx-2 (train) dataset. Even though the method [22] achieved a statistically significant 95% CI, it could achieve only a *fair* quadratic weighted kappa score and a lesser $PPV_{GG>1}$ compared to the proposed method. Only the proposed method and the method in Ref. [22] were able to achieve a statistically significant 95% CI in the grading of PCa into 5 grade groups. The proposed method was able to achieve a *moderate* quadratic weighted kappa score of 0.4727 whereas all other methods could achieve a *fair* quadratic weighted kappa score only. The proposed method as well as the methods in Refs. [21,22] have performed multi-class classification techniques for the prediction of clinically-significant PCa, whereas the other methods have used binary classification techniques. The proposed method cannot be applied to the PROSTATEx-1 dataset, as the same contains ground truth corresponding to clinically significant and clinically insignificant cancers only. The proposed method requires a dataset suitable for multi-class classification. The result of the proposed method as well as the methods by Le et al. [18], Wang et al. [19], Abraham et al. [21] and Jensen et al. [23] are based on the cross-validation performed on training data of the respective PROSTATEx challenges, as the ground truth for the PROSTATEx test data are not publicly available. The methods by Fehr et al. [13] and Jensen et al. [23] used textural features, whereas all other methods used deep features with CNN or a sparse autoencoder. The proposed method and the methods by Le et al. [18], Wang et al. [19], Seah et al. [15] and Abraham et al. [22] used CNN extracted features, whereas the method by Abraham et al. [21] used features extracted

Table 8
Comparison with existing techniques.

Method	Dataset	Number of cases	Classification of GG	AUC	$PPV_{GG>1}$	Quadratic Weighted Kappa	Kappa Concordance	95% CI
Fehr et al. [13]	Private	217	$GG = 1$ vs. $GG >= 2$	0.99	–	–	–	–
Seah et al. [15]	PROSTATEx-1	538	$GG = 1$ vs. $GG >= 2$	0.84	–	–	–	–
Le et al. [18]	PROSTATEx-1(train)+ TJPCa	463	$GG = 1$ vs. $GG >= 2$	0.909 -	–	–		
Wang et al. [19]	PROSTATEx-1(train)	201	$GG = 1$ vs. $GG >= 2$	0.962 -	–	–	–	
Jensen et al. [23]	PROSTATEx-2(train)	112	GG 1 vs. rest	0.85	–	–	–	–
		–	GG 2 vs. rest	0.89	–			
		–	GG (1 + 2) vs. rest	0.83	–			
		–	GG 3 vs. rest	0.94	–			
		–	GG (4 + 5) vs. rest	0.86	–			
Abraham et al. [21]	PROSTATEx-2	181	GG 1, 2, 3, 4, 5	–	0.80	0.2772	fair	
Abraham et al. [21]	PROSTATEx-2 (train)	112	GG 1, 2, 3, 4, 5	–	0.8026	0.2326	fair	
Abraham et al. [22]	PROSTATEx-2 (train)	112	GG 1, 2, 3, 4, 5	–	0.8158	0.3772	fair	[0.2111 to 0.5433]
Proposed method	**PROSTATEx-2 (train)**	112	**GG 1, 2, 3, 4, 5**	**-**	**0.91**	**0.4727**	**moderate**	**[0.27755 to 0.66785]**

using a sparse autoencoder. The method by Fehr et al. [13] used the RFE-SVM classifier, Le et al. [18] used the SVM classifier, Jensen et al. [23] used the KNN classifier, and Abraham et al. [22] used the LADTree classifier. The other methods have used either CNN or the Softmax classifier for classification. To the best of our knowledge, no significant works are available in the literature other than the methods described in Refs. [21,22] which utilized a public dataset to classify 3D volumetric PCa lesions from MRI into 5 grade groups using computer-aided techniques.

The method has a few limitations worth mentioning. The Gleason system does not allow the recognition of low aggressive cancers by some precise criteria [43]. Evaluation of histological images of prostate cancer is done in a subjective manner. The subjectivity of cancer grading leads to the significant inter and intra-observer variability [44,45]. Pathologists have usually great difficulties to assess tumor aggressiveness in the case of borderline lesions like Gleason score 3 + 4 and Gleason score 4 + 3. However, there is a system of complexity and diversity measures that allows a quantitative, fully objective evaluation of tumor aggressiveness [43,45–48]. As future work, we propose to develop computer-aided techniques based on the novel system described in Refs. [43,45–48].

MRI also has certain drawbacks, due to which it cannot be considered as the gold standard for prostate cancer diagnosis. MRI images are evaluated subjectively using PI- RADS criteria. That system, however, has inter and intra-observer variability. Besides, those cancers that will be identified by MRI are usually detected in part only [49,50]. The experiments were performed on a dataset with very few instances. Training instances were significantly less in grade groups 4 and 5. We have not performed any data augmentation techniques for enhancing the size of the training data. The method was able to correctly predict grade 4 prostate cancer in two instances only. This is due to the lesser number of training samples available for grade 4 PCa. Even if the proposed method achieved a *moderate* quadratic weighted kappa score significantly higher than the existing techniques, the accuracy of the diagnosis still requires improvement before clinical use. As a future work, we propose augmentation of training data so that diagnostic accuracy can be improved.

4. Conclusion

The proposed method was able to classify PCa belonging to different grade groups with a *moderate* quadratic weighted kappa score. It was able to predict clinically significant PCa with a $PPV_{GG>1}$ of 0.91. The method achieved a 95% confidence interval of [0.27755, 0.66785]. The result shows that features extracted using pre-trained VGG- 16 networks in combination with the Ordinal Class Classifier is moderately effective for the grading of PCa. The results achieved using the PROSTATEx-2 dataset is better than the existing techniques. Even though the results are promising, further experiments using more datasets are required to confirm its efficiency. For efficient clinical use, the diagnostic accuracy achieved using the proposed method needs further improvement.

Acknowledgment

We thank AAPM, SPIE, NCI,and Radboud University for providing the dataset of the PROSTATEx-2 2017 challenge. We are thankful to Dr. Anil Prahladan, Assistant Professor of Radiology, Regional Cancer Centre (RCC), Thiruvananthapuram, Kerala, India, for suggesting Computer Aided Prostate Cancer Detection as our research topic. We are thankful to the University of Kerala, India, for granting Bejoy Abraham the University Junior Research Fellowship.

References

[1] Siegel RL, Miller KD, Jemal A. Cancer statistics. CA A Cancer J Clin 2019;69(1): 7–34. 2019.
[2] Epstein JI. Prostate cancer grading: a decade after the 2005 modified system. Mod Pathol 2018;31(S1):S47.
[3] Epstein JI, Zelefsky MJ, Sjoberg DD, Nelson JB, Egevad L, Magi- Galluzzi C, Vickers AJ, Parwani AV, Reuter VE, Fine SW, et al. A con- temporary prostate cancer grading system: a validated alternative to the gleason score. Eur Urol 2016; 69(3):428–35.
[4] Epstein JI, Egevad L, Amin MB, Delahunt B, Srigley JR, Humphrey PA, Committee G, et al. The 2014 international society of urological pathology (isup) consensus conference on gleason grading of prostatic carcinoma: defini- tion of grading patterns and proposal for a new grading system. Am J Surg Pathol 2016;40 (2):244–52.
[5] Washino S, Okochi T, Saito K, Konishi T, Hirai M, Kobayashi Y, Miya- gawa T. Combination of prostate imaging reporting and data system (pi-rads) score and prostate-specific antigen (psa) density predicts biopsy outcome in prostate biopsy näıve patients. BJU Int 2017;119(2):225–33.
[6] Verbeek JF, Bangma CH, Kweldam CF, van der Kwast TH, Kümmerlin IP, van Leenders GJ, Roobol MJ. Reducing unnecessary biopsies while detecting clinically significant prostate cancer including cribriform growth with the erspc rotterdam risk calculator and 4kscore. Urologic oncology: seminars and original investigations, vol. 37. Elsevier; 2019. p. 138–44.
[7] Costa DN, Xi Y, Aziz M, Passoni N, Shakir N, Goldberg K, Francis F, Roehrborn CG, Leon ADd, Pedrosa I. Prospective inclusion of apparent diffusion coefficients in multiparametric prostate mri structured reports: discrimination of clinically insignificant and significant cancers. Am. J. Roentgenol. 2019;212(1):109–16.

[8] Mottet N, Bellmunt J, Bolla M, Briers E, Cumberbatch MG, De Santis M, Fossati N, Gross T, Henry AM, Joniau S, et al. Eau-estro-siog guidelines on prostate cancer. part 1: screening, diagnosis, and local treatment with curative intent. Eur Urol 2017;71(4):618–29.
[9] Tabesh A, Teverovskiy M, Pang H-Y, Kumar VP, Verbel D, Kotsianti A, Saidi O. Multifeature prostate cancer diagnosis and gleason grading of histolog- ical images. IEEE Trans Med Imaging 2007;26(10):1366–78.
[10] Ahmed HU, Bosaily AE-S, Brown LC, Gabe R, Kaplan R, Parmar MK, Collaco-Moraes Y, Ward K, Hindley RG, Freeman A, et al. Diagnostic accu- racy of multi-parametric mri and trus biopsy in prostate cancer (promis): a paired validating confirmatory study. The Lancet 2017;389(10071):815–22.
[11] Ouzzane A, Puech P, Lemaitre L, Leroy X, Nevoux P, Betrouni N, Haber G-P, Villers A. Combined multiparametric mri and targeted biopsies improve anterior prostate cancer detection, staging, and grading. Urology 2011;78(6):1356–62.
[12] Fütterer JJ, Briganti A, De Visschere P, Emberton M, Giannarini G, Kirkham A, Taneja SS, Thoeny H, Villeirs G, Villers A. Can clinically signif- icant prostate cancer be detected with multiparametric magnetic resonance imag- ing? a systematic review of the literature. Eur Urol 2015;68(6):1045–53.
[13] Fehr D, Veeraraghavan H, Wibmer A, Gondo T, Matsumoto K, Vargas HA, Sala E, Hricak H, Deasy JO. Automatic classification of prostate cancer gleason scores from multiparametric magnetic resonance images. Proc Natl Acad Sci 2015;112(46): E6265–73.
[14] Armato SG, Huisman H, Drukker K, Hadjiiski L, Kirby JS, Petrick N, Redmond G, Giger ML, Cha K, Mamonov A, et al. Prostatex challenges for computerized classification of prostate lesions from multiparametric magnetic resonance images. J Med Imaging 2018;5(4):044501.
[15] Seah JC, Tang JS, Kitchen A. Detection of prostate cancer on multiparametric mri. Medical imaging 2017: computer-aided diagnosis, vol. 10134. International Society for Optics and Photonics; 2017. p. 1013429.
[16] Liu S, Zheng H, Feng Y, Li W. Prostate cancer diagnosis using deep learning with 3d multiparametric mri. 2017. arXiv preprint arXiv:1703.04078.
[17] Kitchen A, Seah J. Support vector machines for prostate lesion classification. Medical imaging 2017: computer-aided diagnosis, vol.10134. International Society for Optics and Photonics; 2017. p. 1013427.
[18] Le MH, Chen J, Wang L, Wang Z, Liu W, Cheng K-TT, Yang X. Auto- mated diagnosis of prostate cancer in multi-parametric mri based on multimodal convolutional neural networks. Phys Med Biol 2017;62(16):6497.
[19] Wang Z, Liu C, Cheng D, Wang L, Yang X, Cheng K-T. Automated detection of clinically significant prostate cancer in mp-mri images based on an end-to-end deep neural network. IEEE Trans Med Imaging 2018;37(5):1127–39.
[20] Abraham B, Nair MS. Computer-aided diagnosis of clinically significant prostate cancer from mri images using sparse autoencoder and random forest clas- sifier. Biocybernetics. Biomed. Eng. 2018;38(3):733–44.
[21] Abraham B, Nair MS. Computer-aided classification of prostate cancer grade groups from mri images using texture features and stacked sparse autoencoder. Comput Med Imag Graph 2018;69(2):60–8.
[22] Abraham B, Nair MS. Computer-aided grading of prostate cancer from mri images using convolutional neural networks. J. Intell. Fuzzy Syst. 2019;36(3):2015–24.
[23] Jensen C, Carl J, Boesen L, Langkilde NC, Østergaard LR. Assessment of prostate cancer prognostic gleason grade group using zonal-specific features extracted from biparametric mri using a knn classifier. J Appl Clin Med Phys 2019;20(2):146–53.
[24] Mehrtash A, Sedghi A, Ghafoorian M, Taghipour M, Tempany CM, Wells III WM, Kapur T, Mousavi P, Abolmaesumi P, Fedorov A. Classification of clinical significance of mri prostate findings using 3d convolutional neural networks. Medical imaging 2017: computer-aided diagnosis, vol. 10134. ternational Society for Optics and Photonics; 2017. p. 101342A.
[25] Pérez-Ortiz M, Sáez A, Sánchez-Monedero J, Gutiérrez PA, Hervás- Martínez C. Tackling the ordinal and imbalance nature of a melanoma image classification problem. In: 2016 international joint conference on neural networks (IJCNN), IEEE; 2016. p. 2156–63.
[26] Cardoso JS, Cardoso MJ. Towards an intelligent medical system for the aesthetic evaluation of breast cancer conservative treatment. Artif Intell Med 2007;40(2): 115–26.
[27] Clark K, Vendt B, Smith K, Freymann J, Kirby J, Koppel P, Moore S, Phillips S, Maffitt D, Pringle M, et al. The cancer imaging archive (tcia): main- taining and operating a public information repository. J Digit Imaging 2013;26(6):1045–57.
[28] Litjens G, Debats O, Barentsz J, Karssemeijer N, Huisman H. Computer-aided detection of prostate cancer in mri. IEEE Trans Med Imaging 2014;33(5):1083–92.
[29] G. Litjens, O. Debats, J. Barentsz, N. Karssemeijer, H. Huisman, Cancer imaging archive wiki. URL https://doi.org/10.7937/K9TCIA.2017.MURS5CL.
[30] Valliéres M, Freeman CR, Skamene SR, El Naqa I. A radiomics model from joint fdg-pet and mri texture features for the prediction of lung metastases in soft- tissue sarcomas of the extremities. Phys Med Biol 2015;60(14):5471.
[31] Ker J, Wang L, Rao J, Lim T. Deep learning applications in medical image analysis. IEEE Access 2018;6:9375–89.
[32] Deng J, Dong W, Socher R, Li L-J, Li K, Fei-Fei L. Imagenet: a large-scale hierarchical image database. In: Computer vision and pattern recognition, 2009. CVPR 2009. IEEE conference on, ieee; 2009. p. 248–55.
[33] Minaee S, Abdolrashidiy A, Wang Y. An experimental study of deep convolutional features for iris recognition. In: Signal processing in medicine and biology symposium (SPMB), 2016 IEEE, IEEE; 2016. p. 1–6.
[34] Simonyan K, Zisserman A. Very deep convolutional networks for large-scale image recognition. 2014. p. 1556. arXiv preprint arXiv:1409.
[35] Burdick J, Marques O, Weinthal J, Furht B. Rethinking skin lesion segmentation in a convolutional classifier. J. Digit. Imag. 2017:1–6.
[36] Frank E, Hall M. A simple approach to ordinal classification. In: European conference on machine learning. Springer; 2001. p. 145–56.
[37] Quinlan JR. C4. 5: programs for machine learning. Elsevier; 2014.
[38] Cohen J. Weighted kappa: nominal scale agreement provision for scaled dis-agreement or partial credit. Psychol Bull 1968;70(4):213.
[39] Landis JR, Koch GG. The measurement of observer agreement for categorical data. biometrics; 1977. p. 159–74.
[40] Sim J, Wright CC. The kappa statistic in reliability studies: use, interpretation, and sample size requirements. Phys Ther 2005;85(3):257–68.
[41] Fatourechi M, Ward RK, Mason SG, Huggins J, Schlögl A, Birch GE. Comparison of evaluation metrics in classification applications with imbalanced datasets. In: Machine learning and applications, 2008. ICMLA'08. Seventh in- ternational conference on. IEEE; 2008. p. 777–82.
[42] Akosa J. Predictive accuracy: a misleading performance measure for highly imbalanced data. In: Proceedings of the SAS global forum; 2017.
[43] Waliszewski P. Computer-aided image analysis and fractal synthesis in the quantitative evaluation of tumor aggressiveness in prostate carcinomas. Front. Oncol. 2016;6:110.
[44] Nguyen PL, Schultz D, Renshaw AA, Vollmer RT, Welch WR, Cote K, D'Amico AV. The impact of pathology review on treatment recommendations for patients with adenocarcinoma of the prostate. Urologic oncology: semi- nars and original investigations, vol. 22. Elsevier; 2004. p. 295–9.
[45] Waliszewski P. The quantitative criteria based on the fractal dimensions, entropy, and lacunarity for the spatial distribution of cancer cell nuclei enable identifi-cation of low or high aggressive prostate carcinomas. Front Physiol 2016;7:34.
[46] Waliszewski P. On the stratification of adenocarcinomas into the classes of frac- tal dimension equivalence. In: 2015 20th international conference on control systems and computer science. IEEE; 2015. p. 625–32.
[47] Waliszewski P, Wagenlehner F, Gattenlöhner S, Weidner W. On the relationship between tumor structure and complexity of the spatial distribution of cancer cell nuclei: a fractal geometrical model of prostate carcinoma. The Prostate 2015;75(4): 399–414.
[48] Tanase M, Waliszewski P. On complexity and homogeneity measures in predicting biological aggressiveness of prostate cancer; implication of the cellular automata model of tumor growth. J Surg Oncol 2015;112(8):791–801.
[49] The Ups and Downs of MRI Biopsy. The ups and downs of MRI interrogation of the gland: adventures and limitations of MRI. https://www.youtube.com/watch?v=9ShbJf9hMMY. March 2019, accessed on 16.07.2019.
[50] MRI fusion biopsy. https://www.youtube.com/watch?v=i5CDaQXOQas. May 2018, accessed on 16.07.2019.

Update

Informatics in Medicine Unlocked

Volume 20, Issue , 2020, Page

DOI: https://doi.org/10.1016/j.imu.2020.100435

Informatics in Medicine Unlocked 20 (2020) 100435

Contents lists available at ScienceDirect

Informatics in Medicine Unlocked

journal homepage: http://www.elsevier.com/locate/imu

Erratum regarding missing Declaration of Competing Interest statements in previously published articles

Owing to a Publisher error Declaration/Conflict of Interest statements were not included in the published versions of the following articles, that appeared in previous issues of Informatics in Medicine Unlocked.

The appropriate Declaration/Conflict of Interest statements, provided by the Authors, are included below.

1. The relationship between retinal vessel geometrical changes to incidence and progression of Diabetic Macular Edema (Informatics in Medicine Unlocked; 2019; Vol 16C; Article number: 100,248) https://doi.org/10.1016/j.imu.2019.100248

   Declaration of Competing Intere: The Authors have no interests to declare.

2. A machine learning algorithm to improve patient-centric pediatric cardiopulmonary resuscitation (Informatics in Medicine Unlocked; 2020; Vol 19C; Article number: 100,339) https://doi.org/10.1016/j.imu.2020.100339

   Declaration of interest: The Authors have no interests to declare.

3. Decision support system for diagnosing Rheumatic-Musculoskeletal Disease using fuzzy cognitive map technique (Informatics in Medicine Unlocked; 2019; Vol 18C; Article number: 100,279) https://doi.org/10.1016/j.imu.2019.100279

   Declaration of interest: The Authors have no interests to declare.

4. Channel binary pattern based global-local spatial information fusion for motor imagery tasks (Informatics in Medicine Unlocked; 2020; Vol 20C; Article number: 100,352) https://doi.org/10.1016/j.imu.2020.100352

   Declaration of interest: The Authors have no interests to declare.

5. Classification of malignant and benign tissue with logistic regression (Informatics in Medicine Unlocked; 2019; Vol 16C; Article number: 100,189) https://doi.org/10.1016/j.imu.2019.100189

   Declaration of interest: The Authors have no interests to declare.

6. On parameter interpretability of phenomenological-based semi-physical models in biology (Informatics in Medicine Unlocked; 2019; Vol 15C; Article number: 100,158) https://doi.org/10.1016/j.imu.2019.02.002

   Declaration of interest: The Authors have no interests to declare.

7. Multistage Classifier-Based Approach for Alzheimer's Disease Prediction and Retrieval (Informatics in Medicine Unlocked; 2018 vol 14C; Pages 34–42) https://doi.org/10.1016/j.imu.2018.12.003

   Declaration of interest: The Authors have no interests to declare.

8. A novel somatic cancer gene based biomedical document feature ranking and clustering model (Informatics in Medicine Unlocked; 2019; Vol 16C; Article number: 100,188) https://doi.org/10.1016/j.imu.2019.100188

   Declaration of interest: The Authors have no interests to declare.

9. Developing an ultra-efficient microsatellite discoverer to find structural differences between SARS-CoV-1 and Covid-19 (Informatics in Medicine Unlocked; 2020 vol 19C; Article number: 100,356) https://doi.org/10.1016/j.imu.2020.100356

   Declaration of interest: The Authors have no interests to declare.

10. Patient-specific optimization of mechanical ventilation for patients with acute respiratory distress syndrome using quasi-static pulmonary P–V data (Informatics in Medicine Unlocked; 2018;

DOIs of original article: https://doi.org/10.1016/j.imu.2020.100352, https://doi.org/10.1016/j.imu.2020.100356, https://doi.org/10.1016/j.imu.2019.100248, https://doi.org/10.1016/j.imu.2018.12.003, https://doi.org/10.1016/j.imu.2019.100177, https://doi.org/10.1016/j.imu.2019.100189, https://doi.org/10.1016/j.imu.2019.100256, https://doi.org/10.1016/j.imu.2020.100339, https://doi.org/10.1016/j.imu.2019.100279, https://doi.org/10.1016/j.imu.2019.100188, https://doi.org/10.1016/j.imu.2019.100171, https://doi.org/10.1016/j.imu.2018.06.003, https://doi.org/10.1016/j.imu.2018.12.001, https://doi.org/10.1016/j.imu.2020.100308, https://doi.org/10.1016/j.imu.2019.100184, https://doi.org/10.1016/j.imu.2019.02.002, https://doi.org/10.1016/j.imu.2020.100304.

https://doi.org/10.1016/j.imu.2020.100435

Available online 28 September 2020

Vol 12C; Pages 44–55) https://doi.org/10.1016/j.imu.2018.06.003

Declaration of interest: The Authors have no interests to declare.

11. A technology framework for remote patient care in dermatology for early diagnosis (Informatics in Medicine Unlocked; 2019; Vol 15C; Article number: 100,171) https://doi.org/10.1016/j.imu.2019.100171

Declaration of interest: The Authors have no interests to declare.

12. CBIR System Using Capsule Networks and 3D CNN for Alzheimer's disease Diagnosis (Informatics in Medicine Unlocked; 2018; Vol 14C; Pages 59–68) https://doi.org/10.1016/j.imu.2018.12.001

Declaration of interest: The Authors have no interests to declare.

13. The effect of computerized physician order entry on mortality rates in pediatric and neonatal care setting: Meta-analysis (Informatics in Medicine Unlocked; 2020; Vol 19C; Article number: 100,308) https://doi.org/10.1016/j.imu.2020.100308

Declaration of interest: The Authors have no interests to declare.

14. Identification of the core ontologies and signature genes of polycystic ovary syndrome (PCOS): A bioinformatics analysis. (Informatics in Medicine Unlocked; 2020; Vol 18C; Article number: 100,304) https://doi.org/10.1016/j.imu.2020.100304

Declaration of interest: The Authors have no interests to declare.

15. Balanites aegyptiaca (L.) Del. for dermatophytoses: Ascertaining the efficacy and mode of action through experimental and computational approaches (Informatics in Medicine Unlocked; 2019; Vol 15C; Article number: 100,177) https://doi.org/10.1016/j.imu.2019.100177

Declaration of interest: The Authors have no interests to declare.

16. Barriers and technologies of maternal and neonatal referral system in developing countries: A narrative review (Informatics in Medicine Unlocked; 2019; Vol 15C; Article number: 100,184) https://doi.org/10.1016/j.imu.2019.100184

Declaration of interest: The Authors have no interests to declare.

17. Automated Grading of Prostate Cancer using Convolutional Neural Network and Ordinal Class Classifier (Informatics in Medicine Unlocked; 2019; Vol 17C; Article number: 100,256) https://doi.org/10.1016/j.imu.2019.100256

Declaration of interest: The Authors have no interests to declare.